[Title Page]

1. **Turbulent flame propagation limits of ammonia/methane/air premixed mixture in a constant volume vessel**

2. Author (s) : Genya Hashimoto[1], Khalid Hadi[1,3], Yu Xia[1], Aainaa Hamid[1], Nozomu Hashimoto[1], Akihiro Hayakawa[2] Hideaki Kobayashi[2], Osamu Fujita[1]

[1] *Division of Mechanical and Space Engineering, Hokkaido University, Kita13 Nishi8, Kita-ku, Sapporo 060-8628, Japan*

[2] *Institute of Fluid Science, Tohoku University, 2-1-1 Katahira, Aoba-ku, Sendai, Miyagi, 980-8577, Japan*

[3] *Politekmik Sultan Azlan Shah, Behrang 35950, Perak, Malaysia*

3. Corresponding author information:

Nozomu Hashimoto*

Professor, Hokkaido University,

Kita13 Nishi8, Kita-ku, Sapporo 060-8628, Japan

E-mail address: nozomu.hashimoto@eng.hokudai.ac.jp

Tel.: +81-11-706-6386; Fax: +81-11-706-7841

4. Colloquium :

5. Total length of paper : 6199

6. List word equivalent lengths

Body: 2962

Equations: 251

Reference: 402

Table: 193

Figures: 2391[137 + 220 + 110 + 108 + 146 + 160 + 113 + 169 + 169 + 169 + 160 + 160 + 172 + 169 + 229 (for Fig. 1-15 with captions)]

7. Affirmation to pay color reproduction charges (if applicable) : No

Abstract

Ammonia is one of promising energy carriers that can be directly used as carbon-neutral fuel for combustion applications. However, because of the low-burning velocity of ammonia, it is challenging to introduce ammonia to practical combustors those are designed for general hydrocarbon fuels. One of ways to enhance the combustibility of ammonia is by mixing it with other hydrocarbon fuels, such as methane, with a burning velocity is much higher than the burning velocity of ammonia. In this study, we conducted flame propagation experiments of ammonia/methane/air using a fan-stirred constant volume vessel to clarify the effect of methane addition to ammonia on the turbulent flame propagation limit. From experimental results, we constructed the flame propagation maps and clarified the flame propagation limits. The results show that the flame propagation limits were extended with an increase in mixing a fraction of methane to ammonia. Additionally, ammonia/methane/air mixtures with the equivalence ration of 0.9 can propagate at the highest turbulent intensity, even though the peak of the laminar burning velocity is the fuel-rich side because of the diffusional-thermal instability of the flame surface. Furthermore, the Markstein number of the mixture obtained in this research successfully expressed the strength of the diffusional-thermal instability effect on the flame propagation capability. The turbulence Karlovitz number at the flame propagation limit monotonically increases with the decreasing Markstein number.

---

* Corresponding author: Tel.: +81-11-706-6386. E-mail address: nozomu.hashimoto@eng.hokudai.ac.jp

Keywords: Ammonia; Methane; Turbulent Flame propagation; Lewis number; Markstein number

List of figure captions

1. Introduction

Recently, ammonia has been attracting much attention as an energy carrier of hydrogen, as discussed below. Ammonia has a high hydrogen density, is easily liquefied, and stored at room temperatures when it is pressurized. It is also a carbon-neutral fuel like hydrogen, hence, the direct use of ammonia as a fuel is expected. The fundamental studies of ammonia combustion were once conducted in the late 90s[1,2]. According to the advantages as a carbon-neutral fuel, the fundamental studies of ammonia combustion recently became active again [3,4]. Because of the low-burning velocity and a narrow flammable range of ammonia, the mixed combustion of ammonia and natural gas (CH_4) were examined for gas turbine combustors [5]. To improve gas turbine combustors, combustion characteristics should be clarified. In previous studies, the combustion characteristics of ammonia/methane/air in laminar flow-fields were clarified experimentally and numerically [6]. Additionally, the extinction limits of ammonia/air in turbulent fields were clarified experimentally [7]. However, the combustion characteristics of ammonia/methane/air in turbulent fields are unclarified.

In this study, therefore, the objective is the experimental clarification and evaluation of the combustion characteristics, especially the flame propagation limits of ammonia/methane/air in turbulent fields using a fan-stirred constant volume vessel. The flame propagation maps were constructed from the experimental results.

2. Experimental setup/condition and method

Fig. 1 shows a 3D image of the experimental setup. Experiments were conducted using a constant volume spherical chamber as shown in Fig. 1. The inner diameter of the chamber is 200 mm and the height is 280 mm. The total volume of the chamber is approximately 6.19 L. We used an electric spark to make an ignition by a spark ignitor composed of two stainless steel electrodes with diameters of 1.8 mm. The spark gap was set to 3 mm. In Fig. 1, the actual angle between the electrodes and the optical system of Schlieren photography is approximately 45°. A capacitor discharge ignition (CDI) circuit was adopted for spark ignition. Total spark energy of 2.8 J was discharged to the ignition coil to induce

a spark at the center of the chamber. The chamber has two fans and can make turbulent fields. The two fans were placed on the top and bottom of the chamber with electric motors (Maxon Motor, RE40). Eq. (1) expresses the relationship between the rotational speed of the fans and turbulence intensity by using the data from the PIV method [8,9]. The relationship between the fan speed and the turbulence intensity[8] can be seen in Fig. A in the appendix. In Eq. (1), *u'* [m/s] is the turbulence intensity, and *f* [rpm] is the fan rotation speed.

$$u' = 0.00129f \tag{1}$$

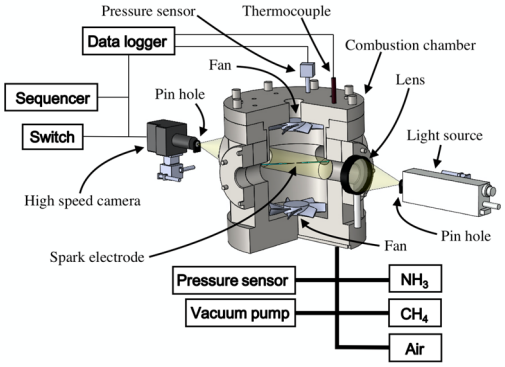

Fig. 1. 3D image of experimental setup

Flame propagations were observed by Schlieren photography using a high-speed camera (Phantom, Miro C210) through a 50-mm-diameter quartz glass window. The resolution of the Schlieren photography was 512 × 512 and the frame rate was 3500 fps.

In this study, three parameters, namely the heat fraction of CH_4 in fuels, E(CH_4), defined by Eq. (2) [6], the equivalence ratio, φ, and the turbulence intensity, *u'*, were varied. In the Eq. (2), *x* is the mole fraction, and *LHV* is the lower heating value. E(CH_4) was set at 0 (NH_3/air), 0.3, 0.7, 1.0 (CH_4/air), the equivalence ratio was varied from 0.4 to 1.7, and the turbulence intensity was 0−5.80 m/s, which is the maximum turbulence intensity of this experimental setup.

$$E(CH_4) = \frac{x_{CH_4} LHV_{CH_4}}{x_{CH_4} LHV_{CH_4} + x_{NH_3} LHV_{NH_3}} \tag{2}$$

Two fans made the turbulent field, and their rotation was kept constant during the experiments. Before supplying gases, the chamber was evacuated by a vacuum pump. Then, a predetermined ratio

of air, methane, and ammonia was supplied into the chamber by measuring the partial pressure of each gas using a pressure sensor (Valcom, VPRTF-A4-(-0.1-1MPa)-5, P2). After supplying gases, the fans stirred the mixture, and it was then ignited. After the ignition, the pressure inside the chamber was constant during the observation range, which is limited by the chamber window size, even though the pressure increased after the observation period. (Fig. C (Fig. 3 of ref. [7]) in Appendix). From the experimental results, the flame propagation limit maps of NH_3/CH_4/air were constructed. All the experiments were conducted at least three times under each condition, but at least six times under conditions near the border of the flame propagation limits.

3. Experimental results

3.1 Laminar burning velocity and Markstein number

The images of the laminar spherical propagating flame were obtained by using the Schlieren method. From the images, the radii of the flames were determined and the flame propagation velocity, S_n, was calculated using Eq. (3):

$$S_n = \frac{dr_{sch}}{dt} \tag{3}$$

where r_{sch} is the equivalent radius calculated from the area of the flame image, and t is time. Additionally, the effect of flame stretch must be considered because stretch affects the spherical propagating flames because of curvature. The flame stretch rate, ε, is time dependent and defined by Eq. (4) [10,11,12]:

$$\varepsilon = \frac{1}{A}\frac{dA}{dt} = \frac{2}{r_{sch}}\frac{dr_{sch}}{dt} \tag{4}$$

where A is the area of the spherical flame front. Various correlations between S_n and ε have been proposed. Kelley and Law [13] proposed a non-linear S_n vs. ε relationship, expressed by Eq. (5):

$$\left(\frac{S_n}{S_s}\right)^2 \ln\left(\frac{S_n}{S_s}\right)^2 = -2\frac{L_b\varepsilon}{S_s} \tag{5}$$

where L_b is the burned gas Markstein length, expressing the sensitivity of the laminar burning velocity to the flame stretch rate. The calculation method of L_b is very important in this study because it can significantly affect the flame propagation limit through the diffusional-thermal instability effect as mentioned later. S_s is the unstretched flame propagation velocity, and the unstretched laminar burning velocity, S_l, can be calculated by Eq. (6) [10,11,12]:

$$S_l = \frac{\rho_b}{\rho_u} S_s \tag{6}$$

where ρ_u and ρ_b are the unburned mixture density and burned gas density, respectively. These values were calculated by using the Dandy research group's website at Colorado State University [14]. From Eq. (5), $\ln(S_n)$ and ε/S_n^2 have a linear correlation. An intercept on the $\ln(S_n)$-axis is $\ln(S_s)$ and the inclination is $-S_sL_b$. Therefore, the burned gas Markstein length and the unstretched flame propagation velocity can be obtained from a linear extrapolation of $\ln(S_n)$ vs. ε/S_n^2 plots [15]. The Markstein number, Ma, is defined by Eq. (7) [16]:

$$Ma = \frac{L_b}{\delta_l} \tag{7}$$

where δ_l is the preheat zone thickness of laminar flames, calculated using Eq. (8):

$$\delta_l = \frac{\lambda}{\rho_u c_p S_l} \tag{8}$$

where λ is the thermal conductivity, and c_p is the specific heat. These values were also calculated by the Dandy research group's website at Colorado State University [14]. The unstretched laminar burning velocity, S_l, was calculated from experimental results by using Eq. (5) and (6). Fig. 2 shows the Schlieren images of the ammonia/methane/air mixture flame at φ = 0.8 in laminar fields (u' = 0 m/s) for E(CH_4) = 0.3, 0.7.

Compared to the case of E(CH_4) = 0.7, the flame shape in the case of E(CH_4) = 0.3 was significantly deformed before reaching the window because of the buoyancy effect. Specifically, deformation at the bottom side of the flame is significant in the last image. This significant deformation was observed at the condition of fuel-lean cases in E(CH_4) = 0 and 0.3, where the flame propagation velocity is low

[10]. Fig. 3 shows the relationship between the flame propagation velocity, S_n, and the flame stretch rate, ε, in E(CH_4) = 0.3 at φ = 0.8. Fig. 4 shows the relationship between the flame shape ratio and ε, in the same experiment as Fig. 3. Three periods can be seen in Figs. 3 and 4, namely an ignition affected period, a quasi-steady period, and a buoyancy-affected period. As observed in Fig. 4, the flame shape ratio in the buoyancy-affected period is steeply decreases as ε decreases (as the flame propagates), while that in the quasi-steady period is almost constant. In this buoyancy-affected period, the buoyancy effect affects the measured propagation velocity (Fig. 3). Therefore, only the data in the quasi-steady period were used to calculate the unstretched laminar burning velocity, S_l, and the Markstein number, *Ma*.

Fig. 5 shows unstretched laminar burning velocities. The unstretched laminar burning velocities of Okafor et al. [6] and Hayakawa et al. [10] are also displayed in Fig. 5. From Fig. 5, the peak of the laminar burning velocity is the fuel-rich side or stoichiometric mixture for all conditions. The unstretched laminar burning velocities derived from our study are consistent with that from Okafor et al. On the other hand, discrepancies of the burning velocities between our study and Hayakawa et al.'s study is significant because of the different methods to determine the unstretched burning velocity. As mentioned previously, we employed the non-linear S_n vs. ε relationship as in Eq. (5) to determine the unstretched laminar burning velocity, while Hayakawa et al. employed the classical S_n vs. ε relationship from Markstein [17] as

$$S_S - S_n = L_b \cdot \varepsilon \tag{9}$$

Figs. 6 and 7 show the Markstein numbers as functions of the equivalence ratio calculated using the classical relationship from Markstein [17] and Eq. (5). The values from the classical definitions (Fig. 6) are much higher than that using Eq. (5) (Fig. 7). Okafor et al. [6] concluded that the Markstein number using Eq. (5) is appropriate for mixtures with Lewis number that is close to unity. Therefore, in this study, we used the Markstein number calculated by using Eq. (5).

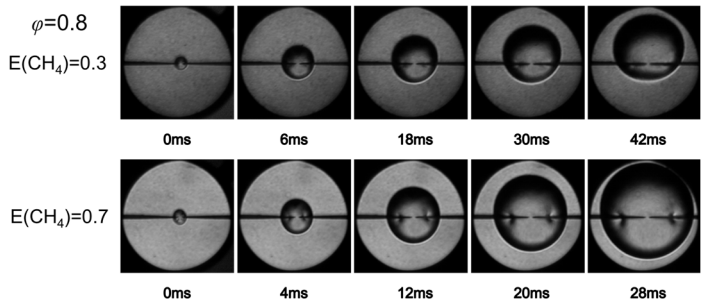

Fig. 2 Schlieren images of the ammonia/methane/air mixture flame at φ = 0.8 in laminar fields (u' = 0 m/s) for E(CH_4) = 0.3, 0.7.

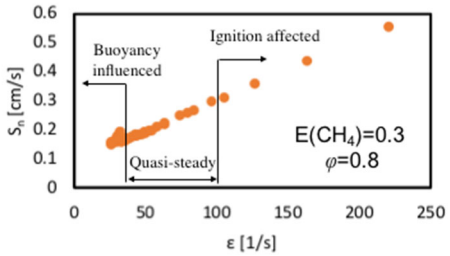

Fig. 3 The relationship between flame propagation velocity, S_n and flame stretch rate, ε.

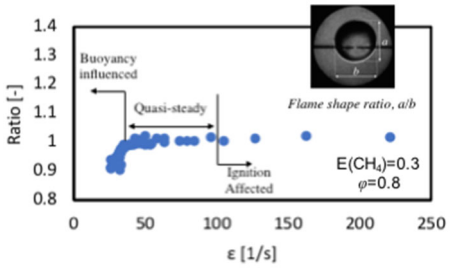

Fig. 4 The variation of flame shape ratio, *a/b*.

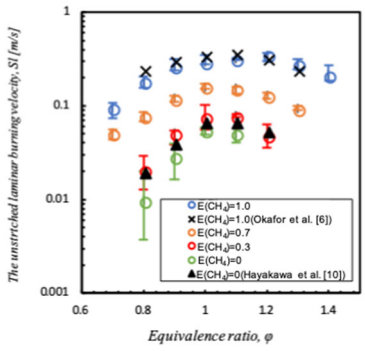

Fig. 5 The unstretched laminar burning velocity as a function of the equivalence ratio.

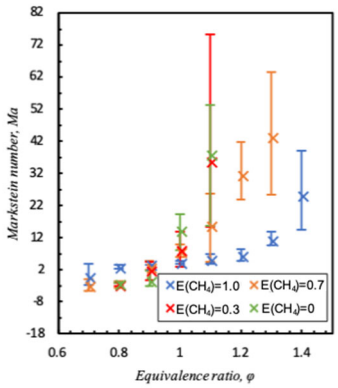

Fig. 6 The Markstein numbers as functions of the equivalence ratio from the classical definition from Markstein[17].

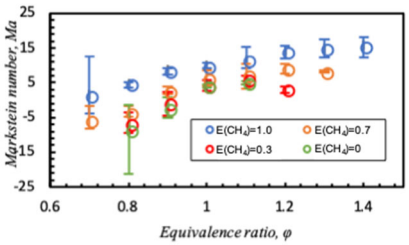

Fig. 7 The Markstein numbers as functions of the equivalence ratio from Eq. (5).

3.2 Flame propagation limits

Figs 8, 9, and 10 show the flame propagation maps on the turbulence intensity vs. the equivalence ratio graphs for E(CH_4) = 0.3, 0.7, and 1.0, respectively. The blue lines indicate the flame propagation limits of NH_3/CH_4/air. The flame propagation limit was defined between the cross marks, ×, in which the propagation probability, p, is 0%, , and the triangle marks, △ (0%< p < 50%) in the maps. In our past study, we concluded that the ignition energy effect is limited to a flame smaller than 8 mm [9] (Fig. B in Appendix). In all the extinction conditions indicated by × in the maps, the flame once reached at the edge of the window with the diameter of a 50 mm. Therefore, the ignition energy did not affect the extinction phenomenon. In the flame propagation cases, the pressure inside the chamber was increased finally (Fig. C in Appendix.). In the extinction cases, however, the pressure inside the chamber was not increased even with the propagation up to its equivalent radius larger than 8 mm, which was defined as the ignition affected radius in the previous research [9] (Fig. B,D in Appendix). The pressure history inside the chamber determined the judgement of extinction or propagation. The black dashed lines indicate the flame propagation limit of NH_3/air from previous research [7]. From these figures, the flame propagation limits were extended with the increase in E(CH_4).

In Figs. 9 and 10 (E(CH_4) = 0.7 and 1.0), the top of the flame propagation limit cannot be seen because of the limitation of the fan speed in the present experimental setup. For E(CH_4) = 1.0, the experiments were conducted only near the border of the flame propagation limit.

In Figs. 8 and 9 (E(CH_4 = 0.3 and 0.7), the flame propagated at the highest turbulence intensity for φ = 0.9, even though the peak of the laminar burning velocity is in the fuel-rich side (Fig. 5). This tendency can also be seen in the flame propagation map for NH_3/air [7], as indicated by the dashed lines in the figures. These tendencies are considered to be due to the Lewis number effect (diffusional-thermal instability), explained later.

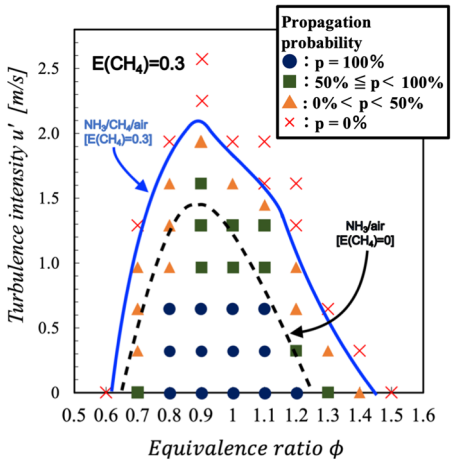

Fig. 8 Flame propagation map for E(CH_4) = 0.3.

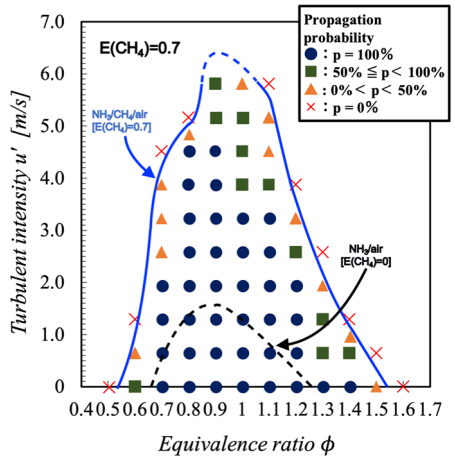

Fig. 9 Flame propagation map for E(CH_4) = 0.7.

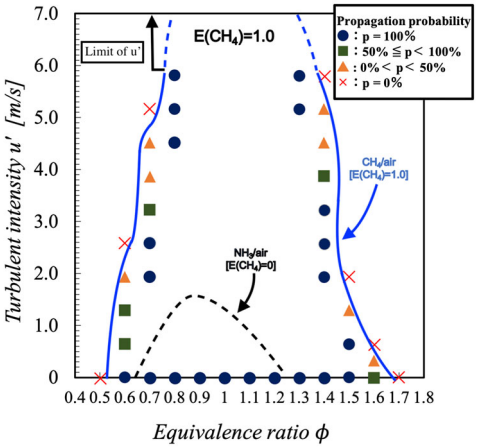

Fig. 10 Flame propagation map for E(CH_4) = 1.0.

3.3 Flame propagation limit maps on turbulence Karlovitz number vs. Markstein number graphs

In order to examine the regimes of the turbulent flames at the propagation limit in this study, all plots in Figs. 8−10 were replotted on the Peters regime diagram in Figs. E−H in Appendix. It was found that the propagation limits were in the various potions in the diagram and it is hard to see clear tendency. Therefore, we introduced the flame propagation maps on the turbulence Karlovitz numbers vs. the Markstein numbers graph as follows.

The turbulence Karlovitz number indicates the relationship between the characteristic time of the chemical reaction and the characteristic time of the disturbance by the turbulent flow. It was calculated by Eq. (10) [18]:

$$Ka = \frac{\delta_l / S_l}{\lambda_f / u'} \tag{10}$$

where λ_f is the longitudinal Taylor microscale , and u' is the turbulence intensity. When the turbulence Karlovitz number is large, the chemical reaction cannot continue at the flame surface, and the flame is extinguished. In previous research, NH_3-air [7], S_l in Eq. (8), is calculated by numerical simulation. However, in this research, S_l is an experimental value.

Figs 11−14 show the flame propagation maps on the turbulence Karlovitz number vs. the Markstein number graphs for E(CH_4) = 0, 0.3, 0.7, and 1.0. The symbols in the figures indicate the same meanings as Figs. 8, 9, and 10, and the dotted lines represent the flame propagation limits. From Figs. 11 to 14, the flames can propagate with a larger turbulence Karlovitz number at a smaller Markstein number, and the turbulence Karlovitz number at the flame propagation limits decreases gradually with the increase of the Markstein number. These tendencies can be also considered to be due to the Lewis number effect.

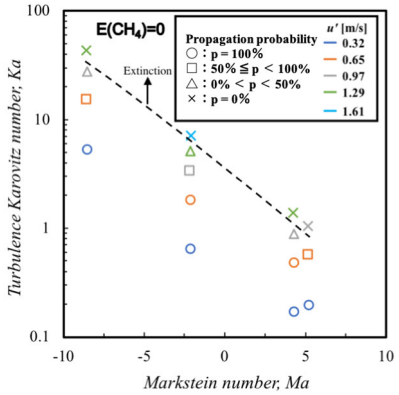

Fig. 11 Flame propagation map in *Ka* vs. *Ma* graph for $E(CH_4) = 0$.

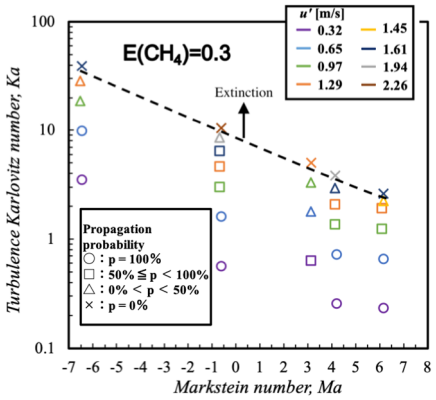

Fig. 12 Flame propagation map in *Ka* vs. *Ma* graph for $E(CH_4) = 0.3$.

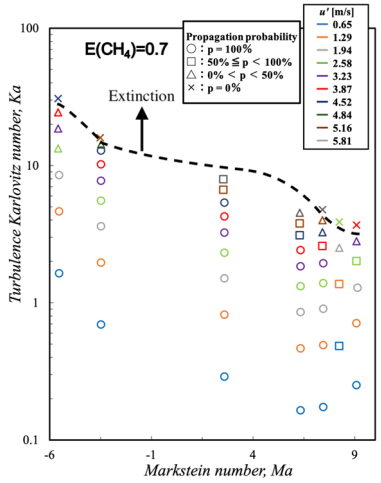

Fig. 13 Flame propagation map in *Ka* vs. *Ma* graph for $E(CH_4) = 0.7$.

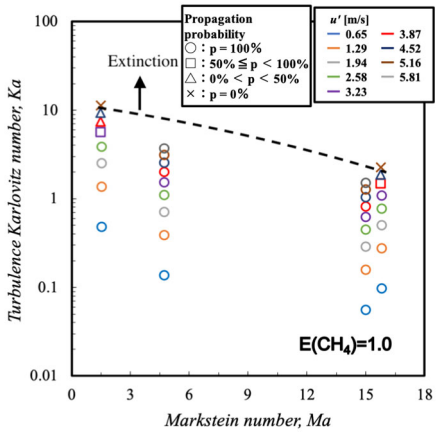

Fig. 14 Flame propagation map in *Ka* vs. *Ma* graph for $E(CH_4) = 1.0$.

n the flame propagation limits

From the flame propagation maps (Figs. 8−10), the flame propagation limits were expanded by adding methane to ammonia. Methane has a higher burning velocity, and a wider flammable range than ammonia.

Consequently, because of adding a highly flammable fuel, methane to ammonia, the flame propagation limits were expanded.

The Markstein number, which is calculated by Eq. (7), is defined as the normalized flame stretch sensitivity [19]. Fig. 11−14 show that the flames cannot propagate with even a small turbulence Karlovitz number in a larger Markstein number compared to in a smaller Markstein number. When the Markstein number is large, the effect of flame stretch becomes larger, and because of the flame stretch, flames easily extinct. Therefore, in larger Markstein numbers, flames cannot propagate with even a small turbulence Karlovitz number.

The Lewis number, *Le*, is, in general, defined as the ratio of the heat diffusivity α and mass diffusivity *D* of deficient reactants. For the two types of fuel mixtures in fuel-lean cases, *Le* is defined by Eq. (11) [20]:

$$Le = x_{NH_3} Le_{NH_3} + x_{CH_4} Le_{CH_4} \tag{11}$$

where *x* is the mole fraction in fuels. Table 1 shows the equivalence ratio and Lewis number for E(CH_4) = 0, 0.3, 0.7, and 1.0. In Table 1, the Lewis number is less than unity for a fuel-lean gas mixture, indicating that mass diffusion is more dominant than thermal diffusion. When the flame surface is deformed by the turbulent eddies and concave and convex shapes are formed, the local burning velocity will be affected by the diffusional-thermal instability. At concave flames, when the Lewis number is less than unity, i.e., the mass diffusion of reactants from the unburned area to the burned area excels the thermal diffusion from the burned area to the unburned area. Consequently, the local temperature and burning velocity in convex areas increase, and a convex shape develops. Alternatively, the local

temperature and burning velocity in concave areas decrease, and a concave shape develops. Eventually, the overall burning velocity increases because of the increase in the flame surface area because of the diffusional-thermal effect originated from the *Le* less than unity. However, when *Le* is larger than unity, the convex and concave structures tend to be suppressed due to the effect opposite to the above effect. Fig. 15 shows the Schlieren images of the ammonia/methane/air mixture for lean (φ = 0.6) and rich (φ = 1.4) fuel conditions in u' = 0.65 m/s for E(CH_4) = 0.7. From Fig. 15, the convex and concave shapes of the flame surface are more developed in the fuel-lean case compared to the fuel-rich case. Because of the increased flame area by the diffusional-thermal instability, the flame propagation velocity increases, and it becomes difficult to extinguish [21]. Although the oxygen concentration condition is different, higher ratio of the turbulent burning velocity to the laminar burning velocity for lean ammonia flame compared to rich ammonia flame in the same turbulence *Ka* was observed in our previous study [9]. Therefore, the flames with an equivalence ratio of 0.9 can propagate in the highest turbulence intensity, as observed in Figs. 8 and 9, even though the peak of the laminar burning velocity is in the fuel-rich side or stoichiometric condition (Fig. 4). We can express the strength of the diffusional-thermal instability effect on the flame propagation capability by the flame propagation maps in Figs. 11−14. The turbulence *Ka* at the flame propagation limit increases with a decreasing *Ma* for all fuel mixtures, as shown in the figures. Even though the values of *Le* for all the mixtures studied are close to the unity (Table 1), the diffusional-thermal instability effect is obvious (Figs. 11−14). There

is a possibility that the hydrogen produced by the decomposition from fuel can promote the diffusional-thermal instability.

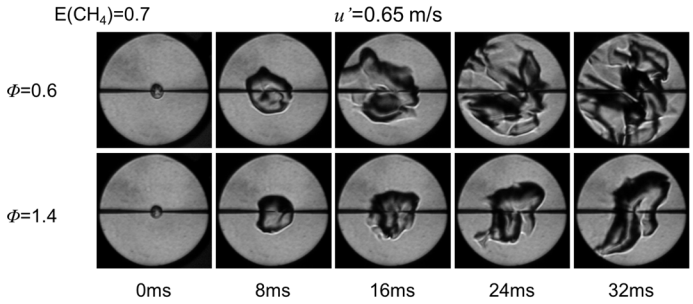

Fig. 15 Schlieren images of ammonia/methane/air mixture flame at fuel-lean and fuel-rich cases in turbulent fields (u' = 0.65m/s) for E(CH_4) = 0.7.

Table 1
Lewis number, *Le*, for E(CH_4) = 0, 0.3, 0.7, and 1.0

φ	0.6	0.7	0.8	0.9	1.0	1.1	1.2	1.3	1.4
E(CH_4)=0	0.955	0.947	0.938	0.930	-	1.097	1.096	1.095	1.094
E(CH_4)=0.3	0.957	0.950	0.941	0.934	-	1.101	1.100	1.100	1.099
E(CH_4)=0.7	0.962	0.956	0.950	0.944	-	1.105	1.105	1.105	1.106
E(CH_4)=1.0	0.970	0.966	0.963	0.960	-	1.106	1.107	1.107	1.108

5. Conclusions

In this study, we conducted flame propagation experiments of ammonia/methane/air using a fan-stirred constant volume vessel to clarify the effect of methane addition to ammonia on the propagation limits of the ammonia/methane/air in turbulent fields. The principal findings are summarized below.

1. The flame propagation limits of ammonia/methane/air are expanded by adding methane to ammonia compared to the pure ammonia flame.
2. The ammonia/methane/air mixture with a 0.9 equivalence ratio can propagate at the highest turbulence intensity, even though the peak of the laminar burning velocity is at the fuel-rich side or stoicheometric condition because of the diffusional-thermal instability of the flame surface.
3. The Markstein number of the mixture obtained in this research successfully expressed the strength of the effect of the diffusional-thermal instability on the flame propagation capability. The turbulence Karlovitz number at the flame propagation limit monotonically increases with a decreasing Markstein number.

Acknowledgment

This work was partly supported by JSPS KAKENHI Grant Number JP19180646 and JST PRESTO Grant No. JPMJPR 1542, the Collaborative Research Project of the Institute of Fluid Science, Tohoku University, and University research support program by Hokkaido Gas Co. Ltd.

References

[1] V. F. Zakaznov, L. A. Kursheva, Z. I. Fedina, Determination of normal flame velocity and critical diameter of flame extinction in ammonia-air mixture, Combustion, Explosion and Shock Waves 14 (1978) 710-713

[2] PD. Ronney, Effect of chemistry and transport properties on near-limit flames as microgravity, Combust. Sci. Tech. 59 (1988) 123-141.

[3] H. Kobayashi, A, Hayakawa, KDKA. Somarathne, EC. Okafor, Science and technology of ammonia combustion, Proc. Combust. Inst. 37 (2019) 109-133.

[4] J. Li, H. Huang, N. Kobayashi, Z. He, Y. Osaka, T. Zeng, Numerical study on effect of oxygen content in combustion air on ammonia combustion, Energy 93 (2) (2015) 2053-2068.

[5] O. Kurata, N. Iki, T. Matsuyama, T. Inoue, T. Tsujimura, H. Furutani, H. Kobayashi, A. Hayakawa, Performances and emission characteristics of NH3-air and NH3-CH4-air combustion gas turbine power generations, Proc. Combust. Inst. 36 (3) (2017) 3351-3359.

[6] E. C. Okafor, Y. Naito, S. Colson, A. Ichikawa, T. Kudo, A. Hayakawa, H. Kobayashi, Experimental and numerical study of the laminar burning velocity of CH4-NH3-air premixed flames, Combust. Flame 187 (2018) 185-198.

[7] Ryo Ichimura, K. Hadi, N. Hashimoto, A. Hayakawa, H. Kobayashi, O. Fujita, Extinction limits of an ammonia/air flame propagating in a turbulent field, Fuel 246 (15) (2019) 178-186.

[8] K. Hadi, R. Ichimura, N. Hashimoto, O. Fujita, Spherical turbulent flame propagation of pulverized coal particle cloud in O2/N2 atomosphere, Proc. Combust. Inst. 37 (3) (2019) 2935-2942.

[9] Y. Xia, G. Hashimoto, K. Hadi, N. Hashimoto, A. Hayakawa, H. Kobayashi, O. Fujita, Turbulent burning velocity of ammonia/oxygen/nitrogen premixed flame in O2-enriched air condition, Fuel 268 (2020) 117383.

[10] A. Hayakawa, T. Goto, R. Mimoto, Y. Arakawa, T. Kudo, H. Kobayashi, Laminar burning velocity and Markstein length of ammonia/air premixed flames at various pressure, Fuel 159 (1) (2015) 98-106.

[11] D. Bradley, RA. Hicks, M. Lawes, CGW. Sheppard, R. Woolley, The mesurement of laminar

burning velocities and markstein numbers for iso-octane-air and iso-octane-n-heptane-air mixtures at elevated temperatures and pressures in an explosion bomb, Combust. Flame 115 (1-2) (1998) 126-144.

[12] A. Hayakawa, Y. Miki, Y. Nagano, T. Kitagawa, Analysis of turbulent burning velocity of spherically propagating premixed flame with effective turbulence intensity, J. Therm. Sci. Technol. 7 (4) (2012) 507-521.

[13] A.P. Kelley, C.K. Law, Nonlinear effects in the extraction of laminar flame speeds from expanding spherical flames, Combust. Flame 156 (9) (2009) 1844-1851.

[14] D. Dandy, Bioanalytical Microfluidics Program, Color. State Univ. n.d., available at <http://navier.engr.colostate.edu/>.

[15] Z. Chen, On the extraction of laminar flame speed and Markstein length from outwardly propagating spherical flames, Combust. Flame 158 (2) (2011) 291-300.

[16] P. Clavin, Dynamic behavior of premixed flame fronts in laminar and turbulent flows, Prog. Energy Combust. Sci. 11 (1) (1985) 1-59.

[17] GH. Markstein, Experimental and theoretical studies of flame-front stability, J. Aerospace Sci. 18 (1951) 199-209.

[18] T. Kitagawa, Y. Nagano, K. Tsuneyoshi, Study on the effects of pressure o turbulent burning velocity of outwardly propagating propane-air flame with turbulence reynolds and markstein numbers, Nihon Kikai Gakkai Ronbunshu, B Hen/Trans. Japan Soc. Mech. Eng. Part B 72 (3) (2006) 825-832.

[19] TC. Lieuwen, Unsteady Combustor Physics, Cambridge University Press, 2012, p. 257-258.

[20] N. Bouvet, F. Halter, C. Chauveau, Y. Yoon, On the effective Lewis number formulations for lean hydrogen/hydrocarbon/air mixtures, Int. J. Hydrogen Energy 38 (14) (2013) 5949-5960.

[21] G. Ciccarelli, S. Dorofeev, Flame acceleration and transition to detonation un ducts, Prog. Energy Combust. Sci. 34 (4) (2008) 499-550